HHS Public Access

Author manuscript

FASEB J. Author manuscript; available in PMC 2021 August 01.

Published in final edited form as:

FASEB J. 2020 August ; 34(8): 10762–10777. doi:10.1096/fj.202000702RR.

Integral role for lysyl oxidase-like-1 in conventional outflow tissue function and behavior

Guorong Li[1,§], **Heather Schmitt**[1,§], **William M. Johnson**[1], **Chanyoung Lee**[2], **Iris Navarro**[1], **Jenny Cui**[3], **Todd Fleming**[1], **Maria Gomez-Caraballo**[1], **Michael H Elliott**[4], **Joseph M. Sherwood**[5], **Michael A. Hauser**[1,6], **Sina Farsiu**[1,7], **C. Ross Ethier**[2,*], **W. Daniel Stamer**[1,7,*]

[1]Department of Ophthalmology, Duke University, Durham, NC, USA

[2]Department of Biomedical Engineering, Georgia Institute of Technology/Emory University, Atlanta, GA, USA

[3]East Chapel Hill School, Chapel Hill, NC, USA

[4]Department of Ophthalmology and Physiology, University of Oklahoma Health, Oklahoma City, OK, USA

[5]Department of Bioengineering. Imperial College London, London, UK

[6]Molecular Physiology Institute, Duke University, Durham, NC, USA

[7]Department of Biomedical Engineering, Duke University, Durham, NC, USA

Abstract

Lysyl oxidase like-1 (LOXL1), a vital crosslinking enzyme in elastin fiber maintenance, is essential for the stability and strength of elastic vessels and tissues. Variants in the LOXL1 locus associate with a dramatic increase in risk of exfoliation syndrome, a systemic fibrillopathy, which often presents with ocular hypertension and exfoliation glaucoma. We examined the role of LOXL1 in conventional outflow function, the prime regulator of intraocular pressure. Using *Loxl1*$^{-/-}$, *Loxl1*$^{+/-}$ and *Loxl1*$^{+/+}$ mice, we observed an inverse relationship between LOXL1 expression and intraocular pressure, which worsened with age. Elevated intraocular pressure in *Loxl1*$^{-/-}$ mice was associated with a larger globe, decreased ocular compliance, increased outflow facility, extracellular matrix abnormalities, and dilated intrascleral veins, yet no dilation of arteries or capillaries. Interestingly, in living *Loxl1*$^{-/-}$ mouse eyes, Schlemm's canal was less susceptible to collapse when challenged with acute elevations in intraocular pressure, suggesting elevated episcleral venous pressure. Thus, LOXL1 expression is required for normal intraocular pressure control, while ablation results in altered extracellular matrix repair/homeostasis and conventional

[*]Corresponding authors W. Daniel Stamer, Ph.D., Duke University, DUMC 3802, 2608 Erwin Rd. Durham, NC 27705, Phone: 919-684-3745, dan.stamer@duke.edu; C. Ross Ethier, Ph.D., Biomedical Engineering, Georgia Institute of Technology, IBB, 315 Ferst Drive, Room 2306, Atlanta, GA 30332-0363, Phone: 404-385-0100, ross.ethier@bme.gatech.edu.

[§]Contributed equally

Author Contributions

G. Li and H. Schmitt designed and performed research, analyzed data, and wrote the paper; W.D. Johnson designed and performed research; C. Lee designed and performed research and analyzed data; I. Navarro, J. Cui, T. Fleming, and M. Gomez-Caraballo performed research; M. Elliot, J.M. Sherwood designed and performed research, analyzed data and wrote segments of the paper; M.A. Hauser designed research and edited the paper; S. Farsiu designed research and analyzed the data; C.R. Ethier and W. D. Stamer designed research, analyzed data, wrote and edited the paper.

outflow physiology. Dilation of Schlemm's canal and distal veins, but not arteries, is consistent with key structural and functional roles for elastin in low-pressure vessels subjected to cyclical mechanical stress.

Keywords

elastin; extracellular matrix; crosslinking; fibrosis; intraocular pressure; Schlemm's canal

Introduction

Lysyl oxidase-like homolog 1 (LOXL1) encodes a member of the lysyl oxidase gene family, which is essential to the biogenesis and repair of extracellular matrix (ECM)-rich connective tissue [39]. Secreted LOXL1 targets to elastin fibers via its pro-region, and then is activated when the pro-region is cleaved by bone morphogenetic protein-1 [5, 52]. Active LOXL1 catalyzes the first step in formation of crosslinks in collagens and elastin [1, 25, 38], playing a critical role in elastic fiber formation, stabilization, maintenance and remodeling [38]. Not surprisingly, LOXL1 is highly expressed in elastic tissues that undergo cycles of mechanical stretch, including lung, aorta and uterus [30, 54, 65, 66].

In the eye, the trabecular meshwork (TM) is a tissue with high elastin content, undergoing repetitive cycles of mechanical stretch; importantly, the TM generates and regulates the majority of aqueous humor outflow resistance, which in turn largely determines intraocular pressure (IOP) [51]. Dysregulation of ECM homeostasis results in ocular hypertension and consequently several types of glaucoma, including primary open-angle glaucoma, primary congenital glaucoma, steroid-induced glaucoma and exfoliation glaucoma (XFG) [2, 14, 32, 37, 42, 61].

XFG is a common ocular consequence of the systemic fibrillopathy known as exfoliation syndrome (XFS) [26]. In fact, XFG is one of the most common types of secondary open-angle glaucoma. XFG is characterized by extracellular exfoliation deposits on visible structures of the eye, such as the crystalline lens and ciliary processes [10]. Significantly, XFG presents with higher IOP at diagnosis and faster progression to blindness than other types of glaucoma [38]. Moreover, XFG has a substantial genetic component. For example, a genome-wide association study showed that three single-nucleotide polymorphisms (SNPs) in the LOXL1 gene strongly associate with the risk of XFG [53]. This finding has been replicated in every population studied to date [1]; however, the contribution of the risk alleles to disease is complicated [1].

Since the specific role of LOXL1 in the pathogenesis of XFG is unclear, transgenic mouse models that overexpress or ablate the *Loxl1* gene have been created [60, 63]. Mice overexpressing LOXL1 protein in the crystalline lens demonstrate higher IOPs at one month of age; however, this phenotype disappears by 3 months [63]. In $Loxl1^{-/-}$ (null) mice on a mixed genetic background (129S1/vj and C57BL/6 background mice), expression of elastin in the TM appeared lower when compared to wild-type C57BL/6 mice, but their IOP phenotype was uncertain because comparisons were made to C57BL/6 wild type mice, not to littermates. $Loxl1^{-/-}$ mice did show a compromised blood–aqueous humor barrier and

formation of cataract, similar to patients with XFG [13, 19, 44, 46, 58]. In addition, decreased LOXL1 gene expression was found in lens capsules of XFG and lamina cribrosa of patients with XFS [15, 43]. Unfortunately, investigators did not phenotype *Loxl1*$^{+/-}$ (heterozygous) mice, which is important since LOXL1 expression levels may have a role in XFG disease progression [45].

Due to these unanswered questions, particularly related to the role of LOXL1 in the elastin-rich TM, we hypothesized that expression level of LOXL1 affects conventional outflow structure and function, and hence IOP. Thus, in addition to IOP measurements in young and old *Loxl1*$^{+/+, +/-, -/-}$ mice, we examined ECM content and conventional outflow tissue anatomy and microanatomy. We also visualized conventional outflow tissue behavior in response to IOP challenges by spectral domain-optical coherence tomography (SD-OCT). Finally, we measured conventional outflow function and ocular compliance using custom perfusion system hardware and software.

Materials and Methods

Animals

Loxl1$^{+/-}$ mice on mixed 129s/ C57BL/6 background were generously provided by Profs. Tiansen Li and Janey Wiggs (Massachusetts Eye and Ear Infirmary/National Institutes of Health). Generation of *Loxl1*$^{-/-}$ mice has been previously described in detail [25]. *Loxl1*$^{+/-}$ mice were inbred to generate *Loxl1* $^{+/+}$ *Loxl1* $^{+/-}$ and *Loxl1*$^{-/-}$ littermates for experiments in this study. C57BL/6 (C57) mice were purchased from the Jackson Laboratory (Bar Harbor, Maine, USA). Animals were handled in accordance with the animal care and use guidelines of Duke University (IACUC animal protocols A020-16-02 and A010-19-01) and in compliance with the ARVO Statement for the Use of Animals in Ophthalmic and Vision Research. The mice were bred/housed in clear cages and kept in housing rooms at 21°C on a 12h:12h light: dark cycle. Mice were divided into 3-4 (young) and 8-12 (aged) month old groups for experiments. As the mice aged past 8 months old, the prevalence of anal prolapse in the *Loxl1*$^{-/-}$ mice increased dramatically, reducing the number of aged animals available for experiments. Therefore, phenotypic reporting for aged mice included animals in the slightly broader age range of 8-12 months to compensate for this loss of animals. Genotyping was performed to identify *Loxl1*$^{-/-}$, *Loxl1* $^{+/-}$ and *Loxl1* $^{+/+}$ mice using primers designed for WT exon 1 (345bp product) and the inserted mutant Neo cassette which introduces a translational STOP codon in exon 1 of the *Loxl1* transcript (~300bp product) (WT FWD: 5'-CGGACCTACGAACAGGGCTACG-3', Mutant FWD: 5'-GAGATCAGCAGCCTCTGTTCCAC-3', and WT/Mutant REV: 5'-ACACGTCGGTGCTGGGATCA-3').

IOP measurements

The mice were anesthetized with ketamine (60 mg/kg) and xylazine (6 mg/kg). IOP was measured immediately upon cessation of movement (i.e., in light sleep) using rebound tonometry (TonoLab, Icare, Raleigh, NC) between 1-2pm [20, 21, 23, 24]. Each recorded IOP was the average of six measurements, giving a total of 36 rebounds from the same eye per recorded IOP value. We were concerned that the *Loxl1* mutation could possibly modify

corneal compliance due to its role in crosslinking elastin and collagens, leading to an error in measured IOP. Thus, the tonometer was calibrated in six eyes of three *Loxl1*$^{-/-}$ mice. Calibration was performed on live, anesthetized animals secured on a platform, following an existing protocol [57]. Briefly, the anterior chamber was cannulated with a glass needle filled with filtered D-glucose in phosphate-buffered saline (DBG, 5.5 mM). The needle was connected to a pressure transducer (px142–001d5v, Omega Engineering, Stamford, CT) whose output was acquired by a PowerLab system (ML870/P PowerLab 8/30, ADInstruments, Colorado Springs, CO), and then to an adjustable-height reservoir containing filtered ddH_2O via 2 stopcocks. IOP was set to either 10, 15, 20, 25, or 30 mmHg by adjusting the reservoir height, and confirmed by readings on the PowerLab system. Before the micropipette was inserted into the anterior chamber, the pressure readings were zeroed to the tear film by placing the needle tip at the same height as its eventual location inside the eye. Tonometer measurements were performed under a microscope to ensure that probe rebounded against the central cornea perpendicularly. Five readings from the tonometer were recorded for each pressure level.

Outflow facility and ocular compliance measurements

Outflow facility and ocular compliance were measured using the iPerfusion system with previously described methods [49]. Littermates (*Loxl1*$^{-/-}$, *Loxl1* $^{+/-}$ and *Loxl1* $^{+/+}$ mice) were euthanized using isoflurane, and eyes were carefully enucleated. Paired eyes were mounted on duplicate stabilization platforms located in the center of perfusion chambers using a small amount of cyanoacrylate glue (Loctite, Westlake Ohio, USA). The perfusion chambers were filled with pre-warmed Dulbecco's phosphate-buffered saline with added 5.5 mM D-glucose, submerging the eyes and regulating temperature at 35°C. Glass microneedles, back filled with filtered DBG, were connected to the system. Using micromanipulators, a microneedle was inserted into the anterior chamber of each eye without contacting the iris. Both eyes were perfused at 9 mmHg for 30 min to allow acclimatization and stabilization, followed by perfusion at 9 sequential pressure steps of 4.5, 6, 7.5, 9, 10.5, 12, 15, 18 and 21 mmHg. Poor quality steps and subsequent pressure steps were eliminated as previously described [49]. Stable flow rate (Q) and pressure (P) averaged over 4 minutes at each pressure step were used for data analysis [23, 24, 49]. A non-linear flow-pressure model ($Q=C_r(P/P_r)^{\beta}P$) that accounts for the pressure-dependence of outflow facility in mice (nonlinearity parameter β), was fit to the flow-pressure data using non-linear regression, yielding the facility C_r evaluated at a reference pressure of P_r = 8 mmHg, which approximates the physiological pressure drop across the conventional outflow pathway in living mice.

Ocular compliance was determined using the volume filling method [48]. System compliance was estimated from a measurement of a glass capillary with hydrodynamic resistance comparable to the outflow pathway in mice. Ocular compliance was calculated for each pressure step and fitted to a modified Friedenwald Equation as described in a previous publication [48]. Only one eye from each pair was analyzed, and where two eyes from a given pair were valid, the eye with the smaller uncertainty on the ocular compliance was selected (indicative of better measurement).

Outliers were removed based on lying more than 2.5 median absolute deviations from the median on the compiled facility and compliance data. Five of 37 eyes were removed based on the compliance outlier criterion. No further eyes were removed due to the facility outlier criterion.

Optical Coherence Tomographic Imaging

In vivo imaging utilized an Envisu R2200 high-resolution spectral domain (SD)-OCT system (Bioptigen Inc., Research Triangle Park, NC). We followed our previously established techniques to image iridocorneal angle structures in mice [6, 20-23]. Briefly, littermates (*Loxl1*$^{-/-}$, *Loxl1*$^{+/-}$ and *Loxl1*$^{+/+}$ mice) were anesthetized with ketamine/xylazine (100 mg/kg and 10 mg/kg) and maintained with ketamine (60 mg/kg) every 20 min by IP administration. While mice were secured in a custom-made platform, a single pulled glass micro-needle filled with phosphate buffered saline (PBS) was inserted into the anterior chamber of one eye. The micro-needle was connected to both a manometric column to adjust IOP and a pressure transducer to continuously monitor IOP levels using PowerLab software. The OCT imaging probe was aimed at the nasal or temporal limbus and the image was centered and focused on the SC lumen. While collecting images, mouse eyes were subjected to a series of IOP steps (10, 12, 15, 17 and 20 mmHg) by adjusting the height of the fluid reservoir. At each IOP step, a sequence of repeated OCT B-scans (each with 1000 A-scans spanning 0.5 mm in lateral length) from spatially close positions was captured, registered, and averaged to create a high signal-to-noise-ratio image from the iridocorneal angle region of each animal.

For pilocarpine experiments, untreated eyes were imaged sequentially at each pressure step, and then the IOP was set back to 10 mm Hg for 10 minutes. A drop of 1% pilocarpine was then given to the mouse single eye, and after a 10 minute wait, the eyes were subjected to the same pressure sequence as before, with images captured at each pressure level.

Segmentation of OCT images

OCT B-scans of iridocorneal angle tissues were registered and segmented following established methods [22, 23] using SchlemmSeg software as previously described in detail [22, 23]. Briefly, OCT B-scans were automatically registered using our custom Schlemm I software for SC segmentation. The Schlemm II software package was then used to differentiate SC from scleral vessels, which were automatically marked. If SC was seen connected to collector channels (CC), manual separation of SC from CC was required, which was based on the shape of SC and speckling in the images [11, 12, 20, 23, 28, 36]. The speckle variance OCT-angiography images were generated based on the speckling in SC and vessels as described in detail in previous publications [22, 23].

Segmentation Reproducibility

To test the reproducibility of the SC segmentation process, we evaluated both inter- and intra-observer reproducibility. The segmentation of SC was independently performed by two individuals. The first observer (GL) conducted the experiments and made initial measurements, then repeated the measurements two to four months after the first examination to determine intra-observer reproducibility. The second observer (either JC or

MGC) was first given a training set of images to evaluate, then reviewed the images for the present study in a masked fashion to assess the inter-observer reproducibility. The inter- and intra-observer reproducibility for quantifying SC lumen area using the semiautomated SchlemmSeg software were 98.1 ± 1.2% and 96.3 ± 2.8%, respectively.

Gross ocular anatomy and lens weights

To determine whether a specific genotype of mouse developed bupthalmia or misshapen eyes over time, aged littermate mice were imaged using a digital camera while each mouse was under anesthesia (for *Loxl1*$^{+/+}$ and *Loxl1*$^{+/-}$ mice, 4 animals per group; for *Loxl1*$^{-/-}$ mice, 3 animals). Post euthanasia, whole globes were imaged on a metric ruler, and eyes were measured using the length measurement tool, scaled to millimeters by the ruler in the image, in ImageJ software (9 month old mice, n=1 per genotype). After dissection, lenses were removed and fixed in 4% paraformaldehyde for 24 hours before being transferred to PBS. Lenses were then measured using the method above (9 month old mice, n=1 per genotype), and lenses were weighed after drying using a Mettler Toledo XS204 scale (*Loxl1*$^{+/+}$ n=12 eyes (6 mice), *Loxl1*$^{+/-}$ n=12 eyes (6 mice), *Loxl1*$^{-/-}$ n=8 eyes (4 mice)).

Histology, Immunohistochemistry and Transmission Electron Microscopy

Eyes from 3 to 12 month old mice were enucleated after euthanasia with isoflurane and immersion fixed in 4% paraformaldehyde at 4 °C overnight. The eyes were then bisected, and the posterior segments and lenses were removed. The anterior segments were cut into four quadrants. For gross morphology studies of outflow tissues, each quadrant was embedded in Epon, and 0.5 μm semi-thin sections were cut, stained with 1% methylene blue and examined by light microscopy (Axioplan2, Carl Zeiss MicroImaging, Thornwood, NY). For immunostaining, each quadrant was embedded in paraffin and 10 μm sections were cut, deparaffinized through xylene and ethanol washes, subjected to a 100°C sodium citrate (pH=6) antigen retrieval step, and immunostained with antibodies that specifically recognized collagen IV (1: 50 dilution, ab6586, rabbit polyclonal, Abcam, Cambridge, MA) and tropoelastin/elastin (1:50 dilution, ab21610, rabbit polyclonal, Abcam, Cambridge, MA). The secondary antibodies were AnffiniPure Goat Anti-Rabbit or mouse IgG H&L (Alexa Fluor® 488; Jackson ImmunoResearch Laboratories, West Grove, PA) at 1:250-1:1,000 dilution. Images were captured using a Nikon Eclipse 90i confocal laser-scanning microscope (Melville, NY, USA). For elastin-collagen staining, 10 μm paraffin sections were deparaffinized and stained with Weigert's Resorcin-Fuschin stain and Van Gieson's stain with hematoxylin nuclear stain (101411-292 to −300, MWBE, Chicago, IL). For electron microscopy studies, mouse anterior segments were embedded in Epon resin and 65 nm ultrathin sagittal sections were cut through iridocorneal tissues using an ultramicrotome (LEICA EM UC6, Leica Mikrosysteme GmbH, A-1170, Wien, Austria). Sections were stained with uranyl acetate/lead citrate and examined with a JEM-1400 electron microscope (JEOL USA, Peabody, MA).

For vessel measurements in anterior segment whole mounts, mouse eyes fixed with 4% paraformaldehyde were hemisected and anterior segment wholemounts were prepared as previously described [7, 18]. Anterior segments were permeabilized with 1% Triton X-100 in phosphate-buffered saline (PBS), blocked with 10% normal horse serum in 0.1% Triton

X-100 in PBS, and incubated with the primary antibody Armenian Hamster monoclonal anti-CD31 (clone 2H8; 1:100; Developmental Studies Hybridoma Bank, University of Iowa) at 4 °C overnight. After washing with 0.1% Triton X-100 in PBS (3 × 20 min), wholemounts were incubated with the appropriate fluorophore-conjugated secondary antibodies (1:500; Life Technologies, Carlsbad, CA, USA and/or Jackson ImmunoResearch Laboratories, West Grove, PA, USA) at 4 °C overnight. After another round of washing (3 X 20 min) with 0.1% Triton X-100 in PBS, 4 radial incisions were made in the anterior segments for flat-mounting in glycerol : PBS (1:1, v/v). Imaging was performed using the Nikon C2si confocal laser scanning microscope (Nikon, Japan), and images were processed with Adobe Photoshop CC 2019 (Adobe Systems, San Jose, CA, USA). Limbal arterioles were distinguishable from limbal venules by endothelial morphology (polarity of CD31 immunoreactivity showing alignment of endothelial cells parallel to longitudinal vessel profile). Limbal capillary loops were easily identifiable as they have small caliber lumens, connect arterioles to venules, and were devoid of alpha smooth muscle actin immunoreactivity. Vessel diameters were measured using ImageJ by applying a grid and measuring vessel widths at each point where a grid line crossed the vessel. Individual vessel measurements were averaged to give an average vessel width per whole mount image.

Statistical analysis

For IOP data analysis, averaged data from both eyes were counted as a single data point for subsequent data analysis. IOP data and data from OCT images were analyzed using ANOVA and the two-side unpaired Students *t*-test. To analyze outflow facility and ocular compliance measurements, we used the well-established fact that the underlying distribution of outflow facility in mice is log-normally distributed [48, 49]. For analysis of compliance and facility, analysis was carried out using R. We first log-transformed the data, consistent with previous studies [48, 49]. The Shapiro-Wilk test did not reject normality for any groups for either variable. Two-way independent ANOVAs were applied to evaluate the effects of genetic background and age on compliance and facility. Tukey's HSD post-hoc test was applied to ascertain pairwise differences between genetic backgrounds. Levene's test was used to evaluate equality of variances, yielding p=0.77 for facility and p=0.05 for compliance. As the latter is borderline significant, which indicates a possible difference in variance between groups, a robust ANOVA and corresponding post-hoc test were carried out using 20% trimmed means. The statistical conclusions from normal and robust ANOVA analyses yielded the same conclusions, hence the former are reported. Data in box and whisker plots show median, 25th percentile, and 75th percentile (boxes), as well as minimum and maximum values (whiskers). Data in other plot formats are presented in the form of mean and 95% confidence interval or mean and standard error of the mean (SEM), as noted. A value of $P \leq 0.05$ was considered statistically significant.

Results

IOP is elevated in *Loxl1*$^{-/-}$ mice.

IOP measurements were conducted in young (3 month) and older (8-12 month) *Loxl1*$^{+/+}$, *Loxl1*$^{+/-}$ and *Loxl1*$^{-/-}$ mice on mixed background (Figure 1 and supplementary Figure 2) using rebound tonometry. Significantly, we found that IOP was higher in *Loxl1*$^{-/-}$ vs.

Loxl1$^{+/+}$ mice (young IOP = 18.4 ± 1.58 (mean ± SD) vs. 16.6 ± 1.59 mmHg, n=10-15, p = 0.016; and older IOP = 20.6 ± 0.53 vs. 17.4 ± 1.73 mmHg, n= 5-7, p = 0.011; Figure 1). However, IOPs in *Loxl1*$^{+/-}$ mice were not different from those in *Loxl1*$^{+/+}$ mice (young IOP = 17.4 ± 1.25, n=10, p = 0.21 and older IOP = 18.8 ± 1.41 mmHg, n=6, p = 0.19). Since it has been reported that IOP in *Loxl1*$^{-/-}$ mice was not different from that in wild type C57BL/6 mice [60], we also measured IOP in 3 month-old C57BL/6 mice and found that IOPs were 18.8 ± 1.10 mmHg (n=8). This value was not different from IOP in *Loxl1*$^{-/-}$ mice (p=0.48), but was significantly higher than in *Loxl1*$^{+/+}$ mice (n=14, p=0.001, supplementary Figure 2). Consistent with elevated IOPs, the eyes of *Loxl1*$^{-/-}$ mice appeared larger than in *Loxl1*$^{-/+}$ and *Loxl1*$^{+/+}$ mice (supplementary Figure 3)

In order to determine whether increased IOP in *Loxl1*$^{-/-}$ mice was due to changes in corneal biomechanical properties, we calibrated our rebound tonometer on *Loxl1*$^{-/-}$ mice, direct setting IOP by cannulating the anterior chamber and comparing the set pressure to measurements using rebound tonometry in the same mouse [57]. As shown in supplementary Figure 4, IOP readings from rebound tonometry were not different from true IOPs in all *Loxl1*$^{+/+}$, *Loxl1*$^{+/-}$ and *Loxl1*$^{-/-}$ eyes. These results indicate that *Loxl1* expression levels did not affect rebound tonometry readings of IOP and that the higher IOP measured in *Loxl1*$^{-/-}$ was not an artifact.

Loxl1 knockout mice exhibited enhanced outflow facility and decreased ocular compliance.

In order to test whether the increased IOP in *Loxl1*$^{-/-}$ mice corresponds to a decrease in outflow function, outflow facility measurements were conducted in young (2-5 month-old) and aged (6-12 month-old) mice (Figure 2A). No effect of age on outflow facility was detected (p=0.98), and there was no interaction between age and genetic background (p=0.93). However, there was a statistically significant effect of genetic background on outflow facility, F(2,28)=4.7, p=0.02. Unexpectedly, we did not find that outflow facility was decreased in *Loxl1*$^{-/-}$ mice; instead, outflow facility was elevated in *Loxl1*$^{-/-}$ mice by 36 [2, 59]% compared to *Loxl1*$^{+/-}$ mice (p=0.05), and by 61 [4, 149]% compared to *Loxl1*$^{+/+}$mice.

We also measured ocular compliance, finding a significant age effect, with ocular compliance being 26 [19, 32]% higher in young than in aged animals (F(2,28)=45.8, p=<10^{-6}; Figure 2B). We observed no interaction between age and genetic background (p=0.59), but found a significant effect of genetic background alone (F(2,28)=3.4, p=0.04), with lower compliance in *Loxl1*$^{-/-}$ mice compared to *Loxl1*$^{+/+}$mice (p=0.04) and *Loxl1*$^{+/-}$ mice (p=0.05).

Schlemm's canal and distal veins are dilated in *Loxl1*$^{-/-}$ mice, consistent with elevated EVP

To determine whether anatomical changes were responsible for physiological findings, we examined vessels distal to SC (intrascleral and aqueous veins), which were visualized by CD31 immunostaining in whole mounts of anterior segments. Using established techniques as described in detail in Materials and Methods to quantify diameter of vessels distal to SC, we found that veins, but not arteries or capillaries, were significantly dilated in *Loxl1*$^{-/-}$

mice (cross-sectional area of 26.7±7.8 μm^2) compared to *Loxl1*$^{+/+}$ mice (15.2±4.1 μm^2, p<0.00001). Vessel diameter in *Loxl1*$^{+/-}$ mice (16.4±2.8 μm^2) was not different from that in *Loxl1*$^{+/+}$ mice (p=0.20, Figure 3).

In addition, outflow tissue structures were visualized by both light microscopy of histological sections and SD-OCT of living eyes. Not surprisingly, due to the abundance of elastin and collagens in the outflow tissue, depletion of *Loxl1* modified outflow tissue structure. As shown in Figure 4, a dramatically enlarged SC lumen in *Loxl1*$^{-/-}$ mice was detected at the light microscopic level in fixed tissue (A-C) and in living animals by SD-OCT (D-F and D'-F'). Quantitative measurements of cross-sectional area of SC lumen by semi-automatic segmentation of OCT images showed that SC area was increased by 3.0 fold in *Loxl1*$^{-/-}$ (5.6 ± 0.7 mm^2, n=11) when compared to *Loxl1*$^{+/+}$ (1.9 ± 0.2 mm^2, n=10, p=0.0001) mice. SC area in *Loxl1*$^{+/-}$ mice (1.8 ± 0.1 mm^2, n=10) was not significant different from that in *Loxl1*$^{+/+}$ mice (p=0.9).

All together, we examined eyes from 22 *Loxl1*$^{-/-}$, 22 *Loxl1*$^{+/-}$ and 22 *Loxl1*$^{+/+}$ mice using 4 different techniques. In every case, we observed an enlarged SC in *Loxl1*$^{-/-}$ mice, relative to *Loxl1*$^{+/+}$ mice (Supplementary table 1). In most cases, sampling was 1-2 quadrants/eye except for immunostaining of SC with PECAM-1 in whole mounted anterior segments, where we sampled segments from all four quadrants/eye, together covering c. 28% of SC's total circumference. The above observations are consistent with elevated episcleral pressure (EVP) in *Loxl1*$^{-/-}$ mice. To estimate the magnitude of this putative EVP elevation, we used Goldmann's equation together with our measured IOP and facility values and assumptions about aqueous inflow and unconventional drainage rates (Supplementary materials, Appendix). These calculations strongly indicate that episcleral venous pressure is significantly elevated in *Loxl1*$^{-/-}$ mice (13.5 mmHg vs. 6.3 mmHg in *Loxl1*$^{+/+}$ animals).

Schlemm's canal in LOXL1 knockout mice is more resistant to IOP-induced collapse

In order to visualize how LOXL1 depletion affects TM/SC behavior, living eyes of *Loxl1*$^{-/-}$, *Loxl1*$^{+/-}$ and *Loxl1*$^{+/+}$ littermates were cannulated to control IOP, and imaged by SD-OCT. Due to dysregulation of ECM protein remodeling and increased incidence of organ prolapse in *Loxl1*$^{-/-}$ mice, we expected that SC in these mice should be more susceptible to collapse than in *Loxl1*$^{+/+}$mice. Surprisingly, the opposite was observed: SCs in *Loxl1*$^{-/-}$ mice were instead resistant to IOP-induced collapse. Specifically, at all pressure levels we tested, SC susceptibility to collapse in *Loxl1*$^{-/-}$ mice was significantly different than in *Loxl1*$^{+/+}$ mice (Figure 5, n=10 for *Loxl1*$^{+/+}$ and n=11 for *Loxl1*$^{-/-}$ mice, p=0.01-0.00001 at pressure levels of 12, 15, 17 and 20 mmHg). Although SC area measurements at IOPs of 17 and 20 mmHg were larger in *Loxl1*$^{+/-}$ mice (n=10) compared to *Loxl1*$^{+/+}$ mice, these differences were not statistically significant at either of the pressure levels (p= 0.22 and 0.07 respectively).

Depletion of LOXL1 leads to altered extracellular matrix material distribution in the conventional outflow pathway.

To determine effect of LOXL1 dosage on crosslinking and remodeling of elastic fibers, staining was conducted on sagittal sections of anterior segments from 9-12 month old *Loxl1*$^{-/-}$, *Loxl1*$^{+/-}$ and *Loxl1*$^{+/+}$ mice. The elastin fibers were noticeably disorganized, and

staining was more prominent in the JCT region of the TM in the *Loxl1*$^{-/-}$ and *Loxl1*$^{+/-}$ mice in comparison to *Loxl1*$^{+/+}$ littermates (Figure 6A, arrows). This phenomenon was more easily noticed using immunohistochemistry against elastin/tropoelastin in the outflow pathway, which illustrated brighter and more disorganized labeling of elastin in the TM (Figure 6B, arrows). Tissue sections were also probed with antibodies specific for collagen IV (Figure 6C), a LOXL1 substrate, showing that *Loxl1*$^{-/-}$ and *Loxl1*$^{+/-}$ mice had visibly higher expression of collagen IV in walls of episcleral vessels when compared to *Loxl1*$^{+/+}$ littermates. In addition, we noticed that blood cells were more frequently present in SC of *Loxl1*$^{-/-}$ mice, indicating higher episcleral venous pressure in these animals.

We next examined the ultrastructure of conventional outflow tissues by transmission electron microscopy (TEM) in *Loxl1*$^{-/-}$ mice. We found an obvious thickening of the basal lamina and increased fibrillary deposits beneath the endothelial cells of the SC inner wall in *Loxl1*$^{-/-}$ mice compared to *Loxl1*$^{+/-}$ and *Loxl1*$^{+/+}$ animals (Figure 7). This was in contrast to the basal lamina of the inner wall of SC in *Loxl1*$^{+/+}$ mice, which was composed of a normal-appearing “patchy”, discontinuous layer of ECM.

Pilocarpine is functional in *Loxl1*$^{-/-}$ mice, lowering IOP and enlarging SC

Elastin fibers extending from the ciliary muscle into the TM and SC inner wall are important in physically and functionally connecting these two tissues [33, 34, 40, 41]. Thus, contraction of the longitudinal ciliary muscle induced by topical pilocarpine lowers IOP by increasing outflow facility, which is associated with enlargement of SC lumen [33, 59]. Due to potential disruption of elastin crosslinking/repair in *Loxl1*$^{-/-}$mice, we hypothesized that contraction of the ciliary muscle with pilocarpine in *Loxl1*$^{-/-}$ mice would lead to less efficacious IOP lowering and SC dilation than in *Loxl1*$^{+/+}$ and *Loxl1*$^{+/-}$ mice. Interestingly, this was not the case: as observed previously [20] we found that pilocarpine enlarged SC lumen by a similar amount in *Loxl1*$^{+/+}$, *Loxl1*$^{+/-}$ and *Loxl1*$^{-/-}$ mice (enlargement of 19.1 ± 2.2%, 18.0 ± 5.6% and 19.8 ± 6.4% respectively, compared to cross-sectional area before pilocarpine treatment, n = 3-4 for each group, Figure 8). We then went on to measure IOP following pilocarpine treatment. Due to lack of availability of mixed background *Loxl1*$^{+/+}$, *Loxl1*$^{+/-}$ and *Loxl1*$^{-/-}$ mice, the IOP experiments were conducted in fourth generation C57BL/6 background *Loxl1*$^{+/+}$, *Loxl1*$^{+/-}$ and *Loxl1*$^{-/-}$ littermates. As shown in supplementary Figure 5, pilocarpine effectively lowered IOP in *Loxl1*$^{-/-}$ mice, with the magnitude of pressure lowering being similar to that seen in *Loxl1*$^{+/+}$ and *Loxl1*$^{+/-}$ mice (IOP reduction of 5.0 ± 0.7 mmHg in *Loxl1*$^{+/+}$ mice (n=6), 5.4 ± 1.9 mmHg in *Loxl1*$^{+/-}$ mice (n=4) and 6.9 ± 0.6 mmHg in *Loxl1*$^{-/-}$ mice (n=3) at 2h post-pilocarpine treatments, p = 0.62). These studies indicate that the presence of LOXL1 does not appear to be required for functional connectivity of the ciliary muscle and TM.

Discussion

The present study was designed to rigorously characterize the impact of LOXL1 expression levels on the structure and function of conventional outflow tissues. Our major observation was that the absence of LOXL1 affected multiple aspects of outflow pathway anatomy and physiology. Specifically, *Loxl1*$^{-/-}$ mice demonstrated ocular hypertension, larger eyes,

elevated outflow facility and decreased ocular compliance compared to *Loxl1*$^{+/+}$ littermates. The occurrence of both elevated IOP and elevated outflow facility may at first appear contradictory; however, quantitative analysis suggests that EVP is significantly elevated in *Loxl1*$^{-/-}$ mice, which likely explains the higher IOPs (see below). Further, a significant elevation of EVP is consistent with the observed dilation of the distal venous vasculature, SC lumen, and increased abundance of red blood cells in SC lumen seen in *Loxl1*$^{-/-}$ animals. Examination of the conventional outflow tissues using immunofluorescence and transmission electron microscopy demonstrated significant alterations in ECM abundance and distribution. Since disruption in ECM homeostasis is known to impact IOP in animal models of glaucoma and in humans [56], our results indicate that LOXL1 has a central role in ECM homeostasis and physiology of both the proximal and distal parts of the conventional aqueous outflow pathway.

At first glance, our IOP results appear to differ from a previous study that performed ocular phenotyping of these mice [60], reporting crystalline lens abnormalities and breakdown of the blood-aqueous barrier, but normal IOPs. In fact, our results essentially replicate those of this earlier study. We used mice derived from two breeding pairs heterozygous for LOXL1 on a mixed 129s/C57BL/6 genetic background, kindly provided by investigators from this original study. The comparison group for IOP measurements in the original study was pure C57BL/6 wild type mice, a strain that is known to have relatively high IOPs [29]. We confirmed IOP data from this previous report, finding that IOPs in *Loxl1*$^{-/-}$mice on a mixed background had IOPs not significantly different from C57BL/6 wild type mice (supplementary Figure 2). However, when we compared *Loxl1*$^{-/-}$ mice to their *Loxl1*$^{+/+}$ littermates, IOPs became progressively different with time. Specifically, IOPs were not different in 1-2 month old mice (not shown), but were significantly higher by 3-months-in *Loxl1*$^{-/-}$ mice, with this elevation becoming more pronounced in adult mice (8-12 months). Consistent with these observations, we found that *Loxl1*$^{-/-}$ mice on mixed background had enlarged ocular globes compared to *Loxl1*$^{+/+}$ littermates. This progressive time course of IOP elevation is consistent with a model of ongoing biomechanical insult to tissues of the outflow pathway, and the role of LOXL1 as an elastic tissue repair enzyme [4, 47].

Surprisingly, in *Loxl1*$^{-/-}$ mice, elevated IOP was not due to increased outflow resistance at the level of the juxtacanalicular region of the conventional outflow tract, where the majority of aqueous outflow resistance is generated. Instead, we observed significantly enhanced outflow facilities, i.e. decreased flow resistances, in enucleated eyes from *Loxl1*$^{-/-}$ mice. An advantage of the technique we used to measure outflow facility is that it functionally isolates key elements of the outflow pathway (JCT/inner wall of SC/distal collecting channels), with a minor contribution from uveoscleral outflow. Thus, it appears that decreased outflow resistance in *Loxl1*$^{-/-}$ mice, which normally would suggest a lower IOP, is more than counteracted by other factors, with the net result being elevated IOP in *Loxl1*$^{-/-}$ mice. Indeed, all available evidence points to elevated EVP driving elevated IOP.

Direct measurement of EVP in pigmented mice is technically challenging and imprecise, and thus we relied instead on a variety of complementary indirect methods to estimate EVP in *Loxl1*$^{-/-}$ mice. For example, we consistently observed red blood cells in SC and significant dilation of SC lumen and distal vessels in *Loxl1*$^{-/-}$ mice, all of which are

indicators of distal venous congestion/elevated EVP. These data are consistent with a recent study where visible-light OCT was used to visualize blood reflux into SC in living mouse eyes that had their episcleral venous pressure acutely elevated [64]. Similar to our data, the investigators found that SC was significantly enlarged after episcleral venous pressure elevation. We hypothesize that chronically elevated EVP propagating back into SC over time in *Loxl1*$^{-/-}$ mice led to the dramatic SC enlargement we observed, consistent with our observations of progressive development of ocular hypertension in *Loxl1*$^{-/-}$ mice. To complement our descriptive assessment of EVP, we used the well-established Goldmann equation to estimate that EVP was 13.5 mmHg in *Loxl1*$^{-/-}$ mice, more than double the estimated value in wild-type animals. Parenthetically, we note that this estimate depends on assumptions about aqueous inflow and unconventional drainage rates, and it would be valuable to develop more robust methods to estimate these quantities in mice. Consistent with results in the present study, LOXL1 appears deficient in varicose veins [35], which are subjected to elevated intraluminal pressures, similar to the elevated EVP that likely exists in *Loxl1*$^{-/-}$ mice.

It is intriguing that we observed enlargement of SC, collector channels and episcleral veins, but not limbal arteries, which seems counter-intuitive in view of the higher pressures in the arterial system. However, in this context it is interesting to note that, under normal circumstances in arteries, elastin is primarily responsible for resisting mechanical loads at low pressures, while collagen carries loads at higher pressures [8]. We thus speculate that this preferential structural role of elastin in low pressure systems may render portions of the aqueous outflow pathway (Schlemm's canal, collector channels and episcleral veins) specifically susceptible to remodeling in LOXL1 null mice. Elastin is also critical for tissue homeostasis under repeated cyclic loading, important due to the pulsatile nature of IOP [55] and the resulting large cyclic deformations seen in SC and the collector channel ostia [62]. Indeed, a recent study [16] showed that loss of LOX in mice led to significant hysteresis and energy loss in the aorta over the cardiac cycle. Hysteresis is thought to be one factor associated with permanent structural change (damage and softening) in connective tissues [9], and thus we suggest that physiological systems characterized by low pressures and large cyclic deformations, such as the conventional outflow tract, may be specifically susceptible to LOXL1 alterations and their effects on the elastin component of the extracellular matrix. More specifically, we hypothesize that hysteresis-associated irreversible remodeling of the aqueous outflow pathway in LOXL1-deficient mice may lead to enlargement of SC and distal aqueous-humor conducting pathways. Further studies will be required to investigate this proposed mechanism in the eye, as well as other low-pressure, high-pulsatility systems.

Using functional measurements of TM/SC responses to acute elevations of IOP in living mice, we observed that SC in *Loxl1*$^{-/-}$ mice was more resistant to lumen collapse than in littermates. In previous studies, we used such observations to quantitatively estimate TM stiffness; however, this was not possible here because, as shown in the Appendix (supplementary materials), the collapse of SC due to IOP (Figure 5) depends on both the intrinsic compliance of the TM as well as the distribution of resistance through the outflow system, the latter of which was unknown in *Loxl1*$^{-/-}$ mice (and likely different from that in wild-type animals). Nonetheless, on its face, resistance to collapse suggests a stiffer TM, which would be surprising for several reasons. First, we have shown recently that TM

stiffness positively correlates with outflow resistance [57], yet we found that facility was greater (outflow resistance was lower) in *Loxl1*$^{-/-}$ mice than in *Loxl1*$^{+/+}$mice. Second, a previous study demonstrated that elastin-rich tissues like the vagina in *Loxl1*$^{-/-}$ mice are mechanically weaker than in *Loxl1*$^{+/+}$ mice [3]. Thus, we suggest that the greater resistance to SC collapse seen in *Loxl1*$^{-/-}$ mice was instead due to greater EVP. Because of this complex relationship among TM tissue stiffness, outflow function, EVP and IOP, further studies will be required to better understand this situation, including possibly in vivo outflow facility measurements.

In addition to its presence near SC and distal veins, elastin is abundant in the TM [33]. In order to test the function of the elastin network connecting the ciliary muscle and TM in *Loxl1*$^{-/-}$ mice, we maximally contracted the ciliary muscle with pilocarpine, a potent muscarinic agonist. Pilocarpine lowers IOP by shortening the longitudinal fibers of the ciliary muscle, which in turn pulls on elastin fibers and inserting in the JCT/inner wall anteriorly [33, 40]. This tension opens flow passageways in the TM and enlarges the lumen of SC, increasing outflow facility [40, 41]. Surprisingly, pilocarpine effectively lowered IOP and enlarged SC in *Loxl1*$^{-/-}$ mice to an extent similar to that seen in *Loxl1*$^{+/+}$ littermates (Figure 8, supplementary Figure 4), suggesting LOXL1 is not required for maintenance of elastic tendons between the ciliary muscle and TM. This was unexpected as LOXL1 is a key enzyme involved in elastin fiber maintenance, essential for the stability and strength of elastic vessels and tissues [3, 27].

It was intriguing that ocular compliance in *Loxl1*$^{-/-}$ mice was lower than wild-type littermates. Since ocular compliance increases with eye size, all other factors being equal [48], this observation strongly suggests increased intrinsic tissue mechanical stiffness of the corneoscleral shell in *Loxl1*$^{-/-}$ mice. This was a surprising result, and suggests that improper crosslinking of elastin and collagen in the corneoscleral shell was compensated for by other mechanisms, e.g. increased collagen content. Since scleral stiffness has been postulated to play a role in glaucomatous optic neuropathy [17, 31, 50] it would be of interest to further study pathophysiology of optic nerve head in *Loxl1*$^{-/-}$ mice. Additionally, it seems that the loss of LOXL1 leads to complex, tissue-specific phenotypical changes, consistent with an important role for LOXL1 in connective tissue repair and homeostasis.

In the mouse outflow system, the presence of a single copy of the LOXL1 gene appeared sufficient to maintain ECM homeostasis, tissue architecture and physiology. For example, pelvic organ prolapse was non-existent and outflow facility was in the normal range for heterozygous mice in both age groups, and IOP in heterozygous mice was also not significantly different from littermate wild-type mice. In terms of conventional outflow tissue architecture, *Loxl1*$^{+/-}$ mice did not display changes found in *Loxl1*$^{-/-}$ mice, such as: (i) increased elastin in the TM/SC, (ii) more abundant, disorganized subendothelial deposits in SC's inner wall (iii) dilated SC and distal vessel lumens. The exception was that both *Loxl1*$^{+/-}$ and *Loxl1*$^{-/-}$ mice displayed increased collagen IV expression surrounding episcleral vessels.

In summary, our data implicate LOXL1 as an enzyme critical to conventional outflow structure and function. The absence of LOXL1 led to elevated EVP accompanied by dilated lumens in SC and distal outflow vessels, as well as dysregulated collagen IV and elastin

homeostasis. These changes together led to progressive IOP elevation over time, and thus aqueous outflow dysfunction. Such findings in *Loxl1*$^{-/-}$ mice emphasize the importance of LOXL1 in ECM homeostasis that appears to go awry in humans with XFG, resulting in fibrillary deposits, SC lumen changes and IOP elevation. We therefore suggest that further studies with *Loxl1*$^{-/-}$ mice will be valuable in studying the pathophysiology of, and possible treatments for, exfoliation glaucoma.

Supplementary Material

Refer to Web version on PubMed Central for supplementary material.

Acknowledgements

We thank that Profs. Tiansen Li and Janey Wiggs for providing LOXL1 knockout mice on behalf of the Massachusetts Eye and Ear Infirmary and the National Eye Institute. We thank Ying Hao (Duke Eye Center Core Facility) for preparing histology sections and helping with TEM, and TeddiJo Watkins, Marybeth Groelle and Megan Parker for genotyping LOXL1 mice. We acknowledge funding support from the BrightFocus Foundation, Research to Prevent Blindness Foundation, The Georgia Research Alliance, and NIH grants EY030124, EY030617, EY028608 and EY005722.

Non-standard Abbreviations

LOXL1:	lysyl oxidase-like-1
XFS:	exfoliation syndrome
XFG:	exfoliation glaucoma
SNP:	single nucleotide polymorphisms
TM:	trabecular meshwork
SC:	Schlemm’s canal
SD-OCT:	spectral domain optical coherence tomography
IOP:	intraocular pressure
ECM:	extracellular matrix
EVP:	episcleral venous pressure
CD31:	cluster of differentiation 31/platelet endothelial cell adhesion molecule
JCT:	juxtacanalicular tissue

References

1. Aboobakar IF, Johnson WM, Stamer WD, Hauser MA, and Allingham RR, 'Major Review: Exfoliation Syndrome; Advances in Disease Genetics, Molecular Biology, and Epidemiology', Exp Eye Res, 154 (2017), 88–103. [PubMed: 27845061]
2. Acott TS, and Kelley MJ, 'Extracellular Matrix in the Trabecular Meshwork', Exp Eye Res, 86 (2008), 543–61. [PubMed: 18313051]

3. Alperin M, Debes K, Abramowitch S, Meyn L, and Moalli PA, 'Loxl1 Deficiency Negatively Impacts the Biomechanical Properties of the Mouse Vagina and Supportive Tissues', Int Urogynecol J Pelvic Floor Dysfunct, 19 (2008), 977–86. [PubMed: 18265927]
4. Behmoaras J, Slove S, Seve S, Vranckx R, Sommer P, and Jacob MP, 'Differential Expression of Lysyl Oxidases Loxl1 and Lox During Growth and Aging Suggests Specific Roles in Elastin and Collagen Fiber Remodeling in Rat Aorta', Rejuvenation Res, 11 (2008), 883–9. [PubMed: 18803461]
5. Borel A, Eichenberger D, Farjanel J, Kessler E, Gleyzal C, Hulmes DJ, Sommer P, and Font B, 'Lysyl Oxidase-Like Protein from Bovine Aorta. Isolation and Maturation to an Active Form by Bone Morphogenetic Protein-1', J Biol Chem, 276 (2001), 48944–9. [PubMed: 11684696]
6. Boussommier-Calleja A, Li G, Wilson A, Ziskind T, Scinteie OE, Ashpole NE, Sherwood JM, Farsiu S, Challa P, Gonzalez P, Downs JC, Ethier CR, Stamer WD, and Overby DR, 'Physical Factors Affecting Outflow Facility Measurements in Mice', Invest Ophthalmol Vis Sci, 56 (2015), 8331–9. [PubMed: 26720486]
7. Elliott MH, Ashpole NE, Gu X, Herrnberger L, McClellan ME, Griffith GL, Reagan AM, Boyce TM, Tanito M, Tamm ER, and Stamer WD, 'Caveolin-1 Modulates Intraocular Pressure: Implications for Caveolae Mechanoprotection in Glaucoma', Sci Rep, 6 (2016), 37127. [PubMed: 27841369]
8. Gabriela Espinosa M, Catalin Staiculescu M, Kim J, Marin E, and Wagenseil JE, 'Elastic Fibers and Large Artery Mechanics in Animal Models of Development and Disease', J Biomech Eng, 140 (2018).
9. Ghasemi M, Nolan DR, and Lally C, 'An Investigation into the Role of Different Constituents in Damage Accumulation in Arterial Tissue and Constitutive Model Development', Biomech Model Mechanobiol, 17 (2018), 1757–69. [PubMed: 30058051]
10. Gottanka J, Flugel-Koch C, Martus P, Johnson DH, and Lutjen-Drecoll E, 'Correlation of Pseudoexfoliative Material and Optic Nerve Damage in Pseudoexfoliation Syndrome', Invest Ophthalmol Vis Sci, 38 (1997), 2435–46. [PubMed: 9375560]
11. Hendargo HC, Estrada R, Chiu SJ, Tomasi C, Farsiu S, and Izatt JA, 'Automated Non-Rigid Registration and Mosaicing for Robust Imaging of Distinct Retinal Capillary Beds Using Speckle Variance Optical Coherence Tomography', Biomed Opt Express, 4 (2013), 803–21. [PubMed: 23761845]
12. Huang Q, Zheng Y, Lu M, Wang T, and Chen S, 'A New Adaptive Interpolation Algorithm for 3d Ultrasound Imaging with Speckle Reduction and Edge Preservation', Comput Med Imaging Graph, 33 (2009), 100–10. [PubMed: 19117725]
13. Kanthan GL, Mitchell P, Burlutsky G, Rochtchina E, and Wang JJ, 'Pseudoexfoliation Syndrome and the Long-Term Incidence of Cataract and Cataract Surgery: The Blue Mountains Eye Study', Am J Ophthalmol, 155 (2013), 83–88 e1. [PubMed: 23036566]
14. Kasetti RB, Maddineni P, Patel PD, Searby C, Sheffield VC, and Zode GS, 'Transforming Growth Factor Beta2 (Tgfbeta2) Signaling Plays a Key Role in Glucocorticoid-Induced Ocular Hypertension', J Biol Chem, 293 (2018), 9854–68. [PubMed: 29743238]
15. Khan TT, Li G, Navarro ID, Kastury RD, Zeil CJ, Semchyshyn TM, Moya FJ, Epstein DL, Gonzalez P, and Challa P, 'Loxl1 Expression in Lens Capsule Tissue Specimens from Individuals with Pseudoexfoliation Syndrome and Glaucoma', Mol Vis, 16 (2010), 2236–41. [PubMed: 21139690]
16. Kim J, Staiculescu MC, Cocciolone AJ, Yanagisawa H, Mecham RP, and Wagenseil JE, 'Crosslinked Elastic Fibers Are Necessary for Low Energy Loss in the Ascending Aorta', J Biomech, 61 (2017), 199–207. [PubMed: 28778385]
17. Kimball EC, Nguyen C, Steinhart MR, Nguyen TD, Pease ME, Oglesby EN, Oveson BC, and Quigley HA, 'Experimental Scleral Cross-Linking Increases Glaucoma Damage in a Mouse Model', Exp Eye Res, 128 (2014), 129–40. [PubMed: 25285424]
18. Kizhatil K, Ryan M, Marchant JK, Henrich S, and John SW, 'Schlemm's Canal Is a Unique Vessel with a Combination of Blood Vascular and Lymphatic Phenotypes That Forms by a Novel Developmental Process', PLoS Biol, 12 (2014), e1001912. [PubMed: 25051267]

19. Kuchle M, Vinores SA, Mahlow J, and Green WR, 'Blood-Aqueous Barrier in Pseudoexfoliation Syndrome: Evaluation by Immunohistochemical Staining of Endogenous Albumin', Graefes Arch Clin Exp Ophthalmol, 234 (1996), 12–8. [PubMed: 8750845]

20. Li G, Farsiu S, Chiu SJ, Gonzalez P, Lutjen-Drecoll E, Overby DR, and Stamer WD, 'Pilocarpine-Induced Dilation of Schlemm's Canal and Prevention of Lumen Collapse at Elevated Intraocular Pressures in Living Mice Visualized by Oct', Invest Ophthalmol Vis Sci, 55 (2014), 3737–46. [PubMed: 24595384]

21. Li G, Farsiu S, Qiu J, Dixon A, Song C, McKinnon SJ, Yuan F, Gonzalez P, and Stamer WD, 'Disease Progression in Iridocorneal Angle Tissues of Bmp2-Induced Ocular Hypertensive Mice with Optical Coherence Tomography', Mol Vis, 20 (2014), 1695–709. [PubMed: 25558173]

22. Li G, Lee C, Agrahari V, Wang K, Navarro I, Sherwood JM, Crews K, Farsiu S, Gonzalez P, Lin CW, Mitra AK, Ethier CR, and Stamer WD, 'In Vivo Measurement of Trabecular Meshwork Stiffness in a Corticosteroid-Induced Ocular Hypertensive Mouse Model', Proc Natl Acad Sci U S A, 116 (2019), 1714–22. [PubMed: 30651311]

23. Li G, Mukherjee D, Navarro I, Ashpole NE, Sherwood JM, Chang J, Overby DR, Yuan F, Gonzalez P, Kopczynski CC, Farsiu S, and Stamer WD, 'Visualization of Conventional Outflow Tissue Responses to Netarsudil in Living Mouse Eyes', Eur J Pharmacol, 787 (2016), 20–31. [PubMed: 27085895]

24. Li G, Torrejon KY, Unser AM, Ahmed F, Navarro ID, Baumgartner RA, Albers DS, and Stamer WD, 'Trabodenoson, an Adenosine Mimetic with A1 Receptor Selectivity Lowers Intraocular Pressure by Increasing Conventional Outflow Facility in Mice', Invest Ophthalmol Vis Sci, 59 (2018), 383–92. [PubMed: 29346804]

25. Liu X, Zhao Y, Gao J, Pawlyk B, Starcher B, Spencer JA, Yanagisawa H, Zuo J, and Li T, 'Elastic Fiber Homeostasis Requires Lysyl Oxidase-Like 1 Protein', Nat Genet, 36 (2004), 178–82. [PubMed: 14745449]

26. Liu Y, Schmidt S, Qin X, Gibson J, Hutchins K, Santiago-Turla C, Wiggs JL, Budenz DL, Akafo S, Challa P, Herndon LW, Hauser MA, and Allingham RR, 'Lack of Association between Loxl1 Variants and Primary Open-Angle Glaucoma in Three Different Populations', Invest Ophthalmol Vis Sci, 49 (2008), 3465–8. [PubMed: 18421074]

27. Mackay EH, Banks J, Sykes B, and Lee G, 'Structural Basis for the Changing Physical Properties of Human Pulmonary Vessels with Age', Thorax, 33 (1978), 335–44. [PubMed: 684670]

28. Mariampillai A, Standish BA, Moriyama EH, Khurana M, Munce NR, Leung MK, Jiang J, Cable A, Wilson BC, Vitkin IA, and Yang VX, 'Speckle Variance Detection of Microvasculature Using Swept-Source Optical Coherence Tomography', Opt Lett, 33 (2008), 1530–2. [PubMed: 18594688]

29. Millar JC, Phan TN, Pang IH, and Clark AF, 'Strain and Age Effects on Aqueous Humor Dynamics in the Mouse', Invest Ophthalmol Vis Sci, 56 (2015), 5764–76. [PubMed: 26325415]

30. Nave AH, Mizikova I, Niess G, Steenbock H, Reichenberger F, Talavera ML, Veit F, Herold S, Mayer K, Vadasz I, Weissmann N, Seeger W, Brinckmann J, and Morty RE, 'Lysyl Oxidases Play a Causal Role in Vascular Remodeling in Clinical and Experimental Pulmonary Arterial Hypertension', Arterioscler Thromb Vasc Biol, 34 (2014), 1446–58. [PubMed: 24833797]

31. Norman RE, Flanagan JG, Sigal IA, Rausch SM, Tertinegg I, and Ethier CR, 'Finite Element Modeling of the Human Sclera: Influence on Optic Nerve Head Biomechanics and Connections with Glaucoma', Exp Eye Res, 93 (2011), 4–12. [PubMed: 20883693]

32. O'Callaghan J, Cassidy PS, and Humphries P, 'Open-Angle Glaucoma: Therapeutically Targeting the Extracellular Matrix of the Conventional Outflow Pathway', Expert Opin Ther Targets, 21 (2017), 1037–50. [PubMed: 28952395]

33. Overby DR, Bertrand J, Schicht M, Paulsen F, Stamer WD, and Lutjen-Drecoll E, 'The Structure of the Trabecular Meshwork, Its Connections to the Ciliary Muscle, and the Effect of Pilocarpine on Outflow Facility in Mice', Invest Ophthalmol Vis Sci, 55 (2014), 3727–36. [PubMed: 24833737]

34. Park CY, Lee JK, Kahook MY, Schultz JS, Zhang C, and Chuck RS, 'Revisiting Ciliary Muscle Tendons and Their Connections with the Trabecular Meshwork by Two Photon Excitation Microscopic Imaging', Invest Ophthalmol Vis Sci, 57 (2016), 1096–105. [PubMed: 26968740]

35. Pascual G, Mendieta C, Mecham RP, Sommer P, Bellon JM, and Bujan J, 'Down-Regulation of Lysyl Oxydase-Like in Aging and Venous Insufficiency', Histol Histopathol, 23 (2008), 179–86. [PubMed: 17999374]
36. Poole KM, McCormack DR, Patil CA, Duvall CL, and Skala MC, 'Quantifying the Vascular Response to Ischemia with Speckle Variance Optical Coherence Tomography', Biomed Opt Express, 5 (2014), 4118–30. [PubMed: 25574425]
37. Raghunathan VK, Morgan JT, Chang YR, Weber D, Phinney B, Murphy CJ, and Russell P, 'Transforming Growth Factor Beta 3 Modifies Mechanics and Composition of Extracellular Matrix Deposited by Human Trabecular Meshwork Cells', ACS Biomater Sci Eng, 1 (2015), 110–18. [PubMed: 30882039]
38. Ritch R, 'The Management of Exfoliative Glaucoma', Prog Brain Res, 173 (2008), 211–24. [PubMed: 18929111]
39. Rodriguez C, and Martinez-Gonzalez J, 'The Role of Lysyl Oxidase Enzymes in Cardiac Function and Remodeling', Cells, 8 (2019).
40. Rohen JW, Futa R, and Lutjen-Drecoll E, 'The Fine Structure of the Cribriform Meshwork in Normal and Glaucomatous Eyes as Seen in Tangential Sections', Invest Ophthalmol Vis Sci, 21 (1981), 574–85. [PubMed: 7287347]
41. Rohen JW, Lutjen E, and Barany E, 'The Relation between the Ciliary Muscle and the Trabecular Meshwork and Its Importance for the Effect of Miotics on Aqueous Outflow Resistance. A Study in Two Contrasting Monkey Species, Macaca Irus and Cercopithecus Aethiops', Albrecht Von Graefes Arch Klin Exp Ophthalmol, 172 (1967), 23–47. [PubMed: 4967268]
42. Safari I, Suri F, Haji-Seyed-Javadi R, Yazdani S, and Elahi E, 'The P.Gly61glu Mutation in Cyp1b1 Affects the Extracellular Matrix in Glaucoma Patients', Ophthalmic Res, 56 (2016), 98–103. [PubMed: 26982174]
43. Schlotzer-Schrehardt U, Hammer CM, Krysta AW, Hofmann-Rummelt C, Pasutto F, Sasaki T, Kruse FE, and Zenkel M, 'Loxl1 Deficiency in the Lamina Cribrosa as Candidate Susceptibility Factor for a Pseudoexfoliation-Specific Risk of Glaucoma', Ophthalmology, 119 (2012), 1832–43. [PubMed: 22633114]
44. Schlotzer-Schrehardt U, and Naumann GO, 'Ocular and Systemic Pseudoexfoliation Syndrome', Am J Ophthalmol, 141 (2006), 921–37. [PubMed: 16678509]
45. Schlotzer-Schrehardt U, Pasutto F, Sommer P, Hornstra I, Kruse FE, Naumann GO, Reis A, and Zenkel M, 'Genotype-Correlated Expression of Lysyl Oxidase-Like 1 in Ocular Tissues of Patients with Pseudoexfoliation Syndrome/Glaucoma and Normal Patients', Am J Pathol, 173 (2008), 1724–35. [PubMed: 18974306]
46. Schumacher S, Nguyen NX, Kuchle M, and Naumann GO, 'Quantification of Aqueous Flare after Phacoemulsification with Intraocular Lens Implantation in Eyes with Pseudoexfoliation Syndrome', Arch Ophthalmol, 117 (1999), 733–5. [PubMed: 10369582]
47. Sethi A, Mao W, Wordinger RJ, and Clark AF, 'Transforming Growth Factor-Beta Induces Extracellular Matrix Protein Cross-Linking Lysyl Oxidase (Lox) Genes in Human Trabecular Meshwork Cells', Invest Ophthalmol Vis Sci, 52 (2011), 5240–50. [PubMed: 21546528]
48. Sherwood JM, Boazak EM, Feola AJ, Parker K, Ethier CR, and Overby DR, 'Measurement of Ocular Compliance Using Iperfusion', Front Bioeng Biotechnol, 7 (2019), 276. [PubMed: 31709244]
49. Sherwood JM, Reina-Torres E, Bertrand JA, Rowe B, and Overby DR, 'Measurement of Outflow Facility Using Iperfusion', PLoS One, 11 (2016), e0150694. [PubMed: 26949939]
50. Sigal IA, Flanagan JG, and Ethier CR, 'Factors Influencing Optic Nerve Head Biomechanics', Invest Ophthalmol Vis Sci, 46 (2005), 4189–99. [PubMed: 16249498]
51. Stamer WD, and Clark AF, 'The Many Faces of the Trabecular Meshwork Cell', Exp Eye Res, 158 (2017), 112–23. [PubMed: 27443500]
52. Thomassin L, Werneck CC, Broekelmann TJ, Gleyzal C, Hornstra IK, Mecham RP, and Sommer P, 'The Pro-Regions of Lysyl Oxidase and Lysyl Oxidase-Like 1 Are Required for Deposition onto Elastic Fibers', J Biol Chem, 280 (2005), 42848–55. [PubMed: 16251195]
53. Thorleifsson G, Magnusson KP, Sulem P, Walters GB, Gudbjartsson DF, Stefansson H, Jonsson T, Jonasdottir A, Jonasdottir A, Stefansdottir G, Masson G, Hardarson GA, Petursson H, Arnarsson

A, Motallebipour M, Wallerman O, Wadelius C, Gulcher JR, Thorsteinsdottir U, Kong A, Jonasson F, and Stefansson K, 'Common Sequence Variants in the Loxl1 Gene Confer Susceptibility to Exfoliation Glaucoma', Science, 317 (2007), 1397–400. [PubMed: 17690259]

54. Tjin G, White ES, Faiz A, Sicard D, Tschumperlin DJ, Mahar A, Kable EPW, and Burgess JK, 'Lysyl Oxidases Regulate Fibrillar Collagen Remodelling in Idiopathic Pulmonary Fibrosis', Dis Model Mech, 10 (2017), 1301–12. [PubMed: 29125826]
55. Turner DC, Edmiston AM, Zohner YE, Byrne KJ, Seigfreid WP, Girkin CA, Morris JS, and Downs JC, 'Transient Intraocular Pressure Fluctuations: Source, Magnitude, Frequency, and Associated Mechanical Energy', Invest Ophthalmol Vis Sci, 60 (2019), 2572–82. [PubMed: 31212310]
56. Vranka JA, Kelley MJ, Acott TS, and Keller KE, 'Extracellular Matrix in the Trabecular Meshwork: Intraocular Pressure Regulation and Dysregulation in Glaucoma', Exp Eye Res, 133 (2015), 112–25. [PubMed: 25819459]
57. Wang K, Li G, Read AT, Navarro I, Mitra AK, Stamer WD, Sulchek T, and Ethier CR, 'The Relationship between Outflow Resistance and Trabecular Meshwork Stiffness in Mice', Sci Rep, 8 (2018), 5848. [PubMed: 29643342]
58. Wang L, Yamasita R, and Hommura S, 'Corneal Endothelial Changes and Aqueous Flare Intensity in Pseudoexfoliation Syndrome', Ophthalmologica, 213 (1999), 387–91. [PubMed: 10567872]
59. Wiederholt M, Thieme H, and Stumpff F, 'The Regulation of Trabecular Meshwork and Ciliary Muscle Contractility', Prog Retin Eye Res, 19 (2000), 271–95. [PubMed: 10749378]
60. Wiggs JL, Pawlyk B, Connolly E, Adamian M, Miller JW, Pasquale LR, Haddadin RI, Grosskreutz CL, Rhee DJ, and Li T, 'Disruption of the Blood-Aqueous Barrier and Lens Abnormalities in Mice Lacking Lysyl Oxidase-Like 1 (Loxl1)', Invest Ophthalmol Vis Sci, 55 (2014), 856–64. [PubMed: 24425853]
61. Wordinger RJ, and Clark AF, 'Lysyl Oxidases in the Trabecular Meshwork', J Glaucoma, 23 (2014), S55–8. [PubMed: 25275908]
62. Xin C, Johnstone M, Wang N, and Wang RK, 'Oct Study of Mechanical Properties Associated with Trabecular Meshwork and Collector Channel Motion in Human Eyes', PLoS One, 11 (2016), e0162048. [PubMed: 27598990]
63. Zadravec P, Braunger BM, Melzer B, Kroeber M, Bosl MR, Jagle H, Schlotzer-Schrehardt U, and Tamm ER, 'Transgenic Lysyl Oxidase Homolog 1 Overexpression in the Mouse Eye Results in the Formation and Release of Protein Aggregates', Exp Eye Res, 179 (2019), 115–24. [PubMed: 30399364]
64. Zhang X, Beckmann L, Miller DA, Shao G, Cai Z, Sun C, Sheibani N, Liu X, Schuman J, Johnson M, Kume T, and Zhang HF, 'In Vivo Imaging of Schlemm's Canal and Limbal Vascular Network in Mouse Using Visible-Light Oct', Invest Ophthalmol Vis Sci, 61 (2020), 23.
65. Zhao BH, and Zhou JH, 'Decreased Expression of Elastin, Fibulin-5 and Lysyl Oxidase-Like 1 in the Uterosacral Ligaments of Postmenopausal Women with Pelvic Organ Prolapse', J Obstet Gynaecol Res, 38 (2012), 925–31. [PubMed: 22487196]
66. Zhou Y, Ling O, and Bo L, 'Expression and Significance of Lysyl Oxidase-Like 1 and Fibulin-5 in the Cardinal Ligament Tissue of Patients with Pelvic Floor Dysfunction', J Biomed Res, 27 (2013), 23–8. [PubMed: 23554790]

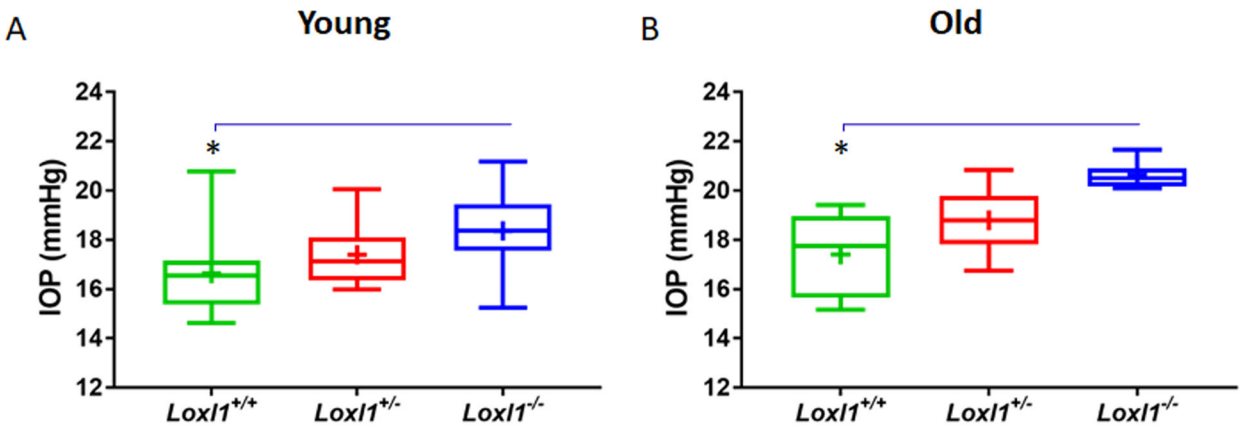

Figure 1. *Loxl1*$^{-/-}$ demonstrate elevated IOPs.

(A) IOPs was measured in age-matched mixed background littermates of *Loxl1*$^{-/-}$, *Loxl1*$^{+/-}$ and *Loxl1*$^{+/+}$ young (3 months, n=10 mice/20 eyes for both *Loxl1*$^{-/-}$ and *Loxl1*$^{+/-}$ mice, n=14 mice/28 eyes for *Loxl1*$^{+/+}$ mice) and **(B)** older (8-12 month old mice (n=7 mice/14 eyes for *Loxl1*$^{-/-}$ mice, n=6 mice/12 eyes for *Loxl1*$^{+/-}$ mice and n=5 mice/10 eyes for *Loxl1*$^{+/+}$ mice) using rebound tonometry under light anesthesia . IOPs were significantly higher in *Loxl1*$^{-/-}$ mice when compared to *Loxl1*$^{+/+}$ mice at 3 and 8-12 months of age (*$p<0.05$). Data are shown as mean ± SD.

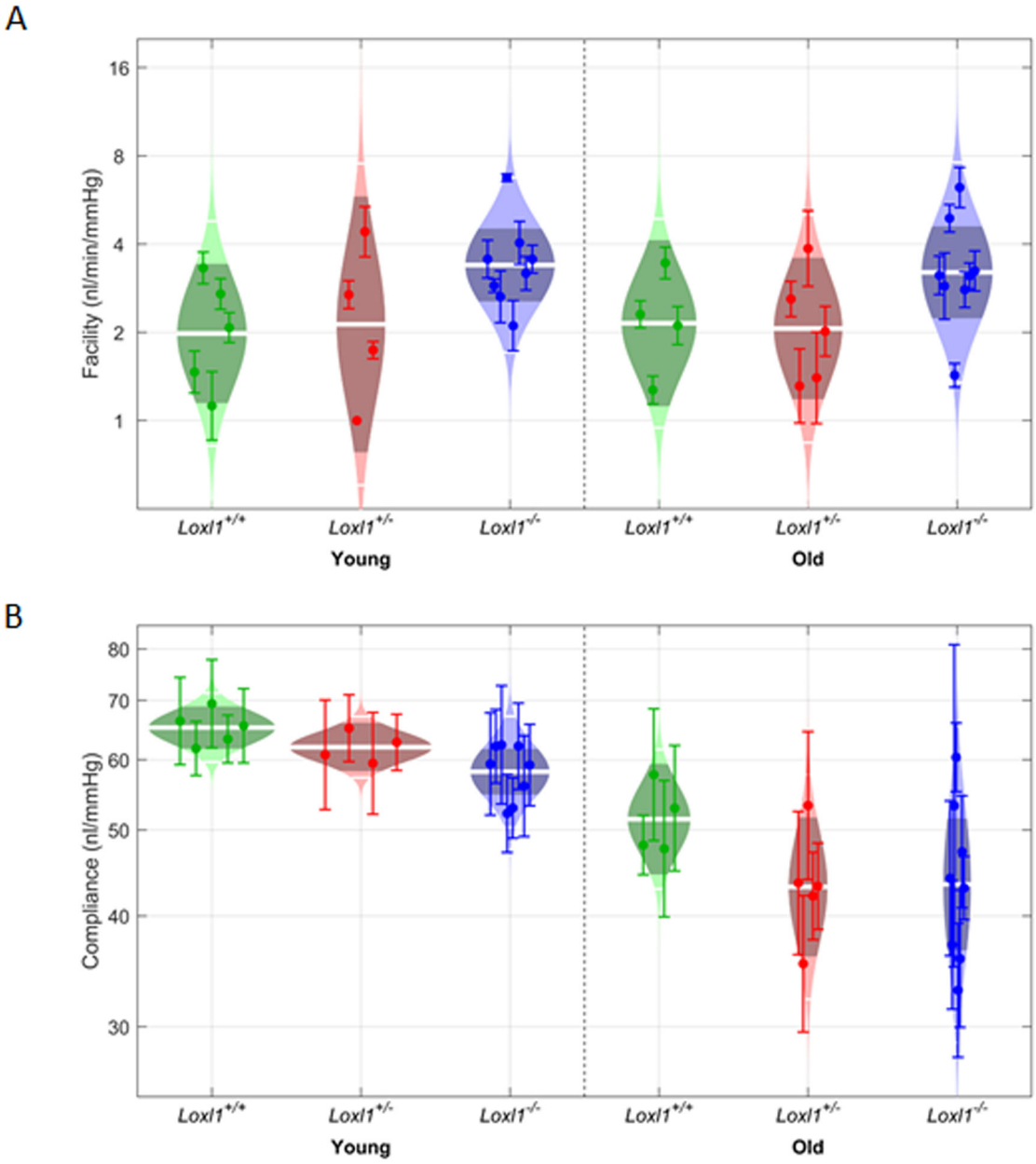

Figure 2. ***Loxl1*** $^{-/-}$ **mice have increased outflow facility and decreased ocular compliance.**
Outflow facility and ocular compliance measurements were conducted in enucleated young (2-5 months) and older (6-12 months) littermates *Loxl1* $^{+/+}$, *Loxl* $^{+/-}$and *Loxl1* $^{-/-}$ mice using iPerfusion. Ocular compliance was also determined during facility measurements following an existing method published previously (1). Panels **(A)** and **(B)** show cello plots for the 6 individual groups for facility and compliance respectively. For cello plot displays, shaded region shows estimated lognormal distribution of facility/compliance. Outer white lines show 2 geometric standard deviations and central lines shows the geometric mean. Dark central band shows the 95% confidence interval on the mean.

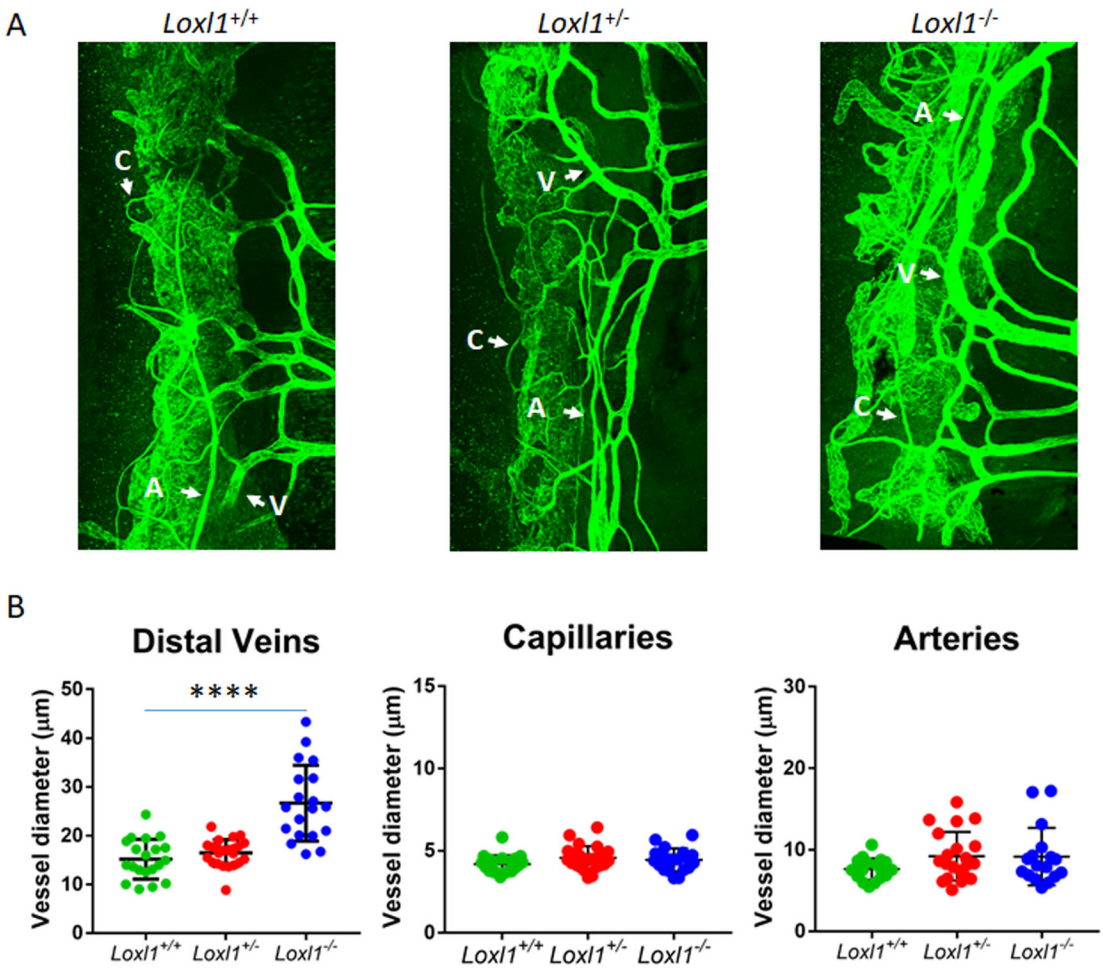

Figure 3. ***Loxl1*$^{-/-}$ mice display dilated distal outflow veins but not arteries or capillaries.**

(A) *Loxl1*$^{-/-}$, *Loxl1*$^{+/-}$ and *Loxl1*$^{+/+}$ mouse anterior segments were immunostained with antibody against CD31, and imaged using confocal microscopy at 20 × magnification. **(B)** Measurements of distal outflow vessels indicate a significant increase in distal vessel width in *Loxl1*$^{-/-}$ mice when compared to *Loxl1*$^{+/+}$ eyes (****p<0.0001). There was no difference between *Loxl1*$^{+/+}$ and *Loxl1*$^{+/-}$ eyes. The central line in the scatter plot indicates the mean (n=6 eyes from 4 mice for both *Loxl1*$^{+/+}$ and *Loxl1*$^{+/-}$, n=6 eyes from 5 mice for *Loxl1*$^{-/-}$) A, arteries; V, veins; C, capillaries (scale bar=100µm).

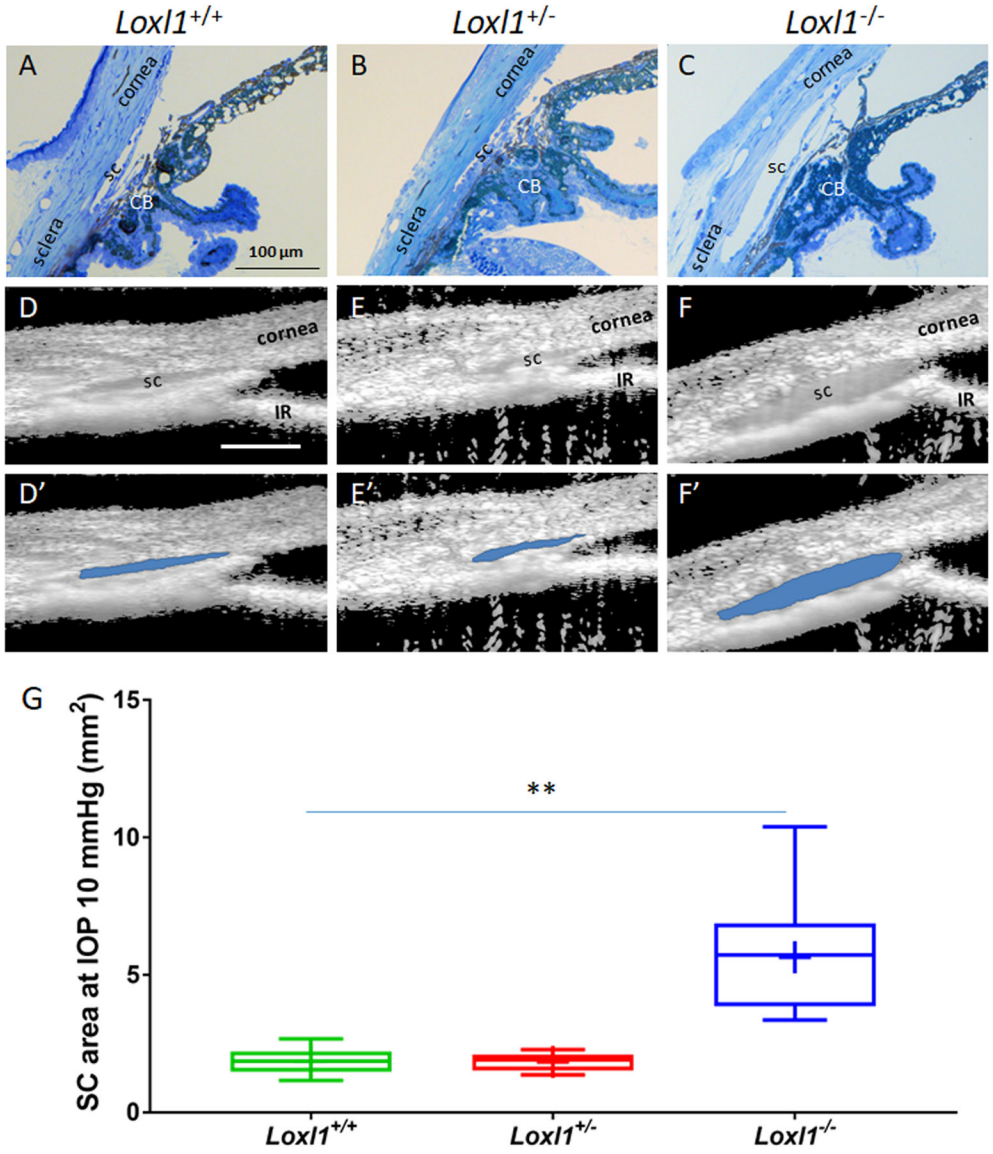

Figure 4. A dramatically enlarged Schlemm's canal lumen is present in *Loxl1*$^{-/-}$ mice.

(A-C) *Loxl1*$^{-/-}$, *Loxl1*$^{+/-}$ and *Loxl1*$^{+/+}$ mouse anterior segments were fixed, sagittally sectioned, stained with methylene blue and imaged (n=3 for *Loxl1*$^{+/+}$ and *Loxl1*$^{+/-}$, n=4 for Loxl1$^{-/-}$). **(D-F)** Cross-sectional images from living *Loxl1*$^{-/-}$, *Loxl1*$^{+/-}$ and *Loxl1*$^{+/+}$ mice were recorded using SD-OCT and SC lumen was segmented using custom software. **(D'-F')** The segmented SC lumen is highlighted in blue corresponding to panels **(D-F)**. **(G)** Quantitative analysis of SC luminal cross-sectional areas indicated a significantly larger SC in the *Loxl1*$^{-/-}$ mice when compared to *Loxl1*$^{+/-}$ mice (**p=0.0001; n=10 eyes for both *Loxl1*$^{+/+}$ and *Loxl1*$^{+/-}$mice, n=11 eyes for *Loxl1*$^{-/-}$mice*).* The central line in box and whisker plots represents the median, the top and bottom edges are 25th and 75th percentiles, the whiskers extend to the most extreme data points not considered outliers and "+" indicates the mean. Scale bar=100µm.

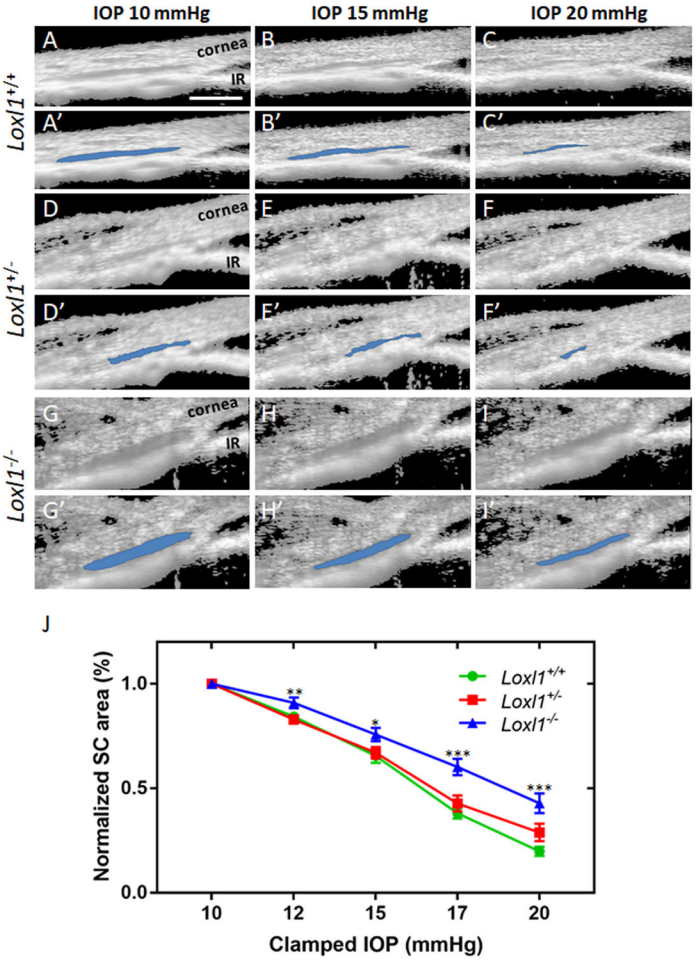

Figure 5. Schlemm's canal in *Loxl1*$^{-/-}$ mice is more resistant to pressure-induced collapse.

(A-I) Living *Loxl1*$^{-/-}$, *Loxl1*$^{+/-}$ and *Loxl1*$^{+/+}$ mouse eyes were cannulated to control IOP and subjected to sequentially increasing pressure steps (10-20 mmHg) while imaging conventional outflow tissues using SD-OCT. **(A'-I')** Images were analyzed and SC lumens were semi-automatically segmented (in blue) using custom software. IR, iris. **(J)** Quantitative comparison of SC lumen areas in *Loxl1*$^{-/-}$, *Loxl1*$^{+/-}$ and *Loxl1*$^{+/+}$ mice at 5 clamped IOPs (10, 12, 15, 17 and 20 mmHg) shows a decreased tendency toward SC collapse in *Loxl1*$^{-/-}$eyes when compared to *Loxl1*$^{+/+}$ eyes (p=0.01-0.00001 at IOPs of 12, 15, 17 and 20 mmHg). Data are shown as mean ± SE values for each IOP (n = 10 for *Loxl1*$^{+/-}$ and *Loxl1*$^{+/+}$ and n = 11 for *Loxl1*$^{-/-}$ mice).

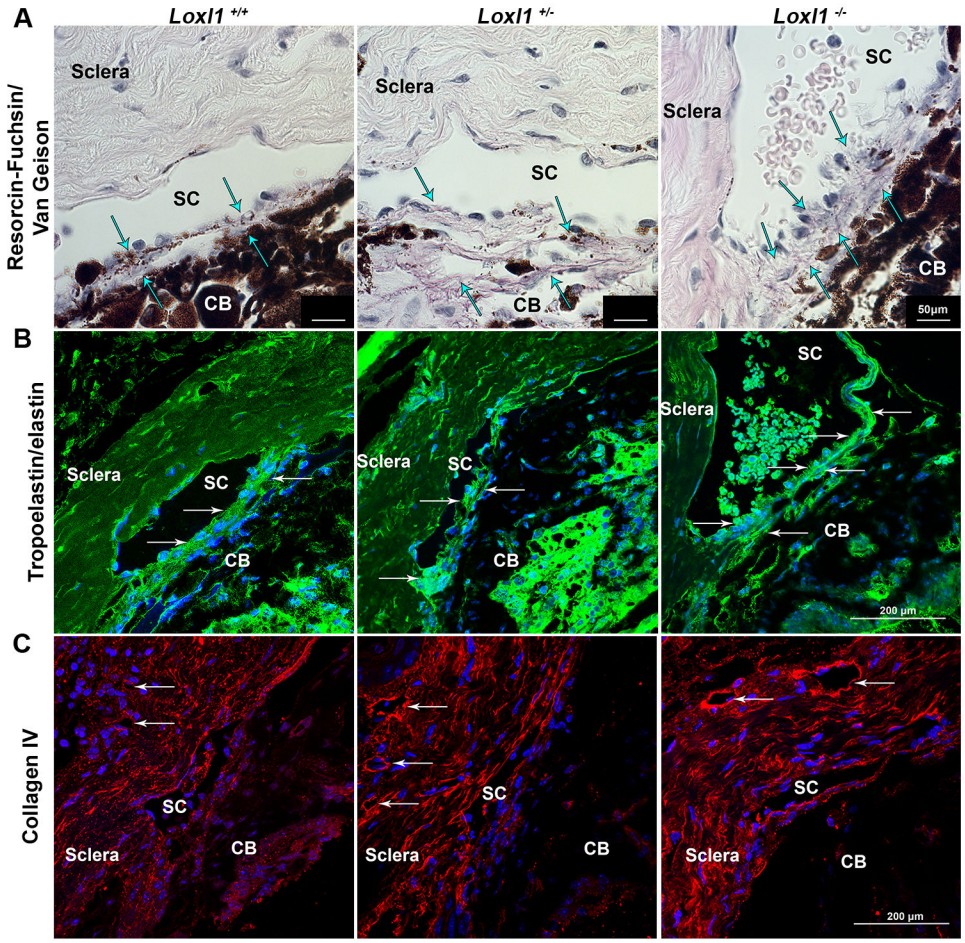

Figure 6. ***Loxl1*** $^{-/-}$ **mice have altered distribution of collagen IV and elastin fibers in the conventional outflow pathway.**

(A) Paraffin sections stained for collagen and elastin show an accumulation of elastin (arrows point to dark purple fibers) in the outflow pathway of *Loxl1*$^{-/-}$ eyes in comparison to *Loxl1*$^{-/+}$ and *Loxl1*$^{+/+}$ eyes, which maintained a longer fiber structure with age (n=3 mice) (scale bar = 50μm). **(B)** Sections from *Loxl1*$^{-/-}$ eyes indicated increased tropoelastin/ elastin immunolabeling in the TM and JCT regions (arrows) in comparison to *Loxl1*$^{-/+}$ and *Loxl1*$^{+/+}$ eyes (n=3 mice) (scale bar=200 μm). **(C)** Sagittal sections from *Loxl1*$^{-/-}$ and *Loxl1*$^{-/+}$ eyes showed increased immunolabeling of collagen IV around distal vessels (arrows) of outflow tissues in comparison to *Loxl1*$^{+/+}$ eyes (n=3 mice) (scale bar=200 μm). Note the blood cells in the lumen of SC in the *Loxl1*$^{-/-}$ eye.

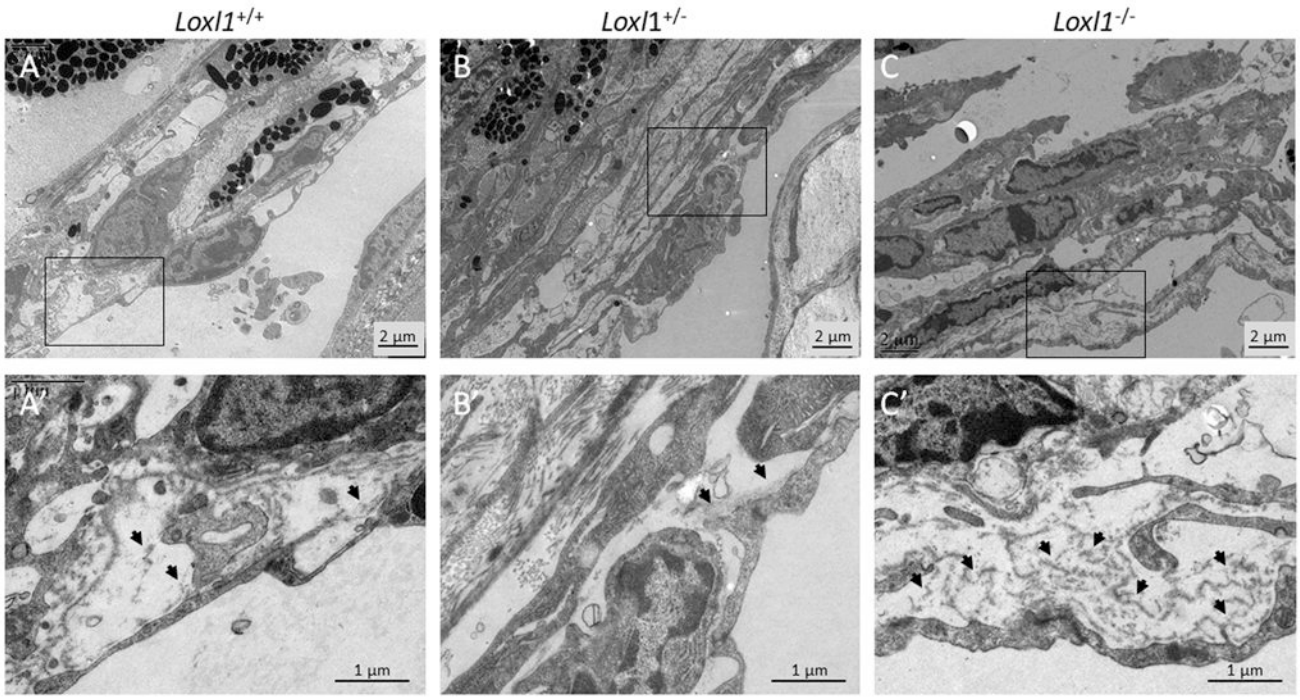

Figure 7. *Loxl1*$^{-/-}$ mice display more basal laminar deposits beneath inner wall SC endothelial cells.

Loxl1$^{-/-}$, *Loxl1*$^{+/-}$ and *Loxl1*$^{+/+}$ mouse anterior segments were embedded in Epon, sectioned, stained with uranyl acetate/lead citrate, and examined with a JEM-1400 electron microscope (JEOL USA). **(A-C)** Representative images from conventional outflow pathway of *Loxl1*$^{-/-}$, *Loxl1*$^{+/-}$ and *Loxl1* $^{+/+}$ eyes. **(A'-C')** show enlarged areas indicated by boxes in **(A-C).** Arrows point to basal laminar material beneath SC endothelial cells. (n=4 *Loxl1*$^{+/+}$ mice, n=4 *Loxl1*$^{+/-}$ mice, n=5 *Loxl1*$^{-/-}$ mice).

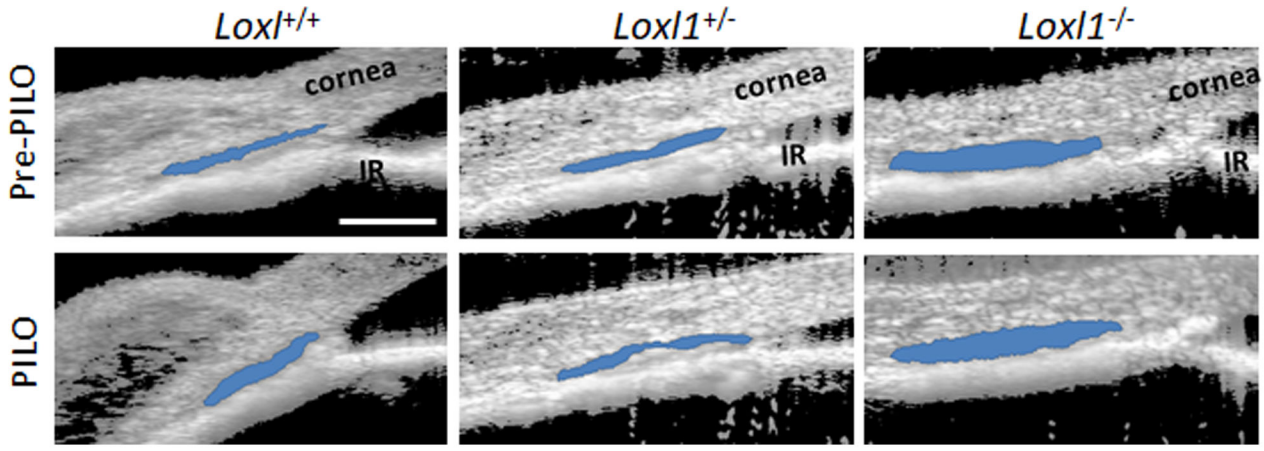

Figure 8. Pilocarpine alters sizes of conventional outflow structures in *Loxl1*$^{-/-}$ mice.

Sagittal sections of mixed background *Loxl1*$^{-/-}$, *Loxl1*$^{+/-}$ and *Loxl1*$^{+/+}$ mouse anterior segments were imaged using SD-OCT at IOP 10 mmHg prior and post topical 1% pilocarpine treatment. SC lumen was segmented using custom software. Data show representative mouse anterior segment OCT images from *Loxl1*$^{-/-}$, *Loxl1*$^{+/-}$ and *Loxl1*$^{+/+}$ mice pre- and post-pilocarpine treatment (n=3 for *Loxl1*$^{+/+}$, n=4 for *Loxl1*$^{+/-}$ and *Loxl1*$^{-/-}$ mice). Segmentation of SC is indicated by blue color. PILO, pilocarpine; IR, iris. Blue area, SC. Scale bar=100μm.